Oxysterol Compounds in Mouse Mutant αA- and αB-Crystallin Lenses Can Improve the Optical Properties of the Lens

Kehao Wang,[1] Masato Hoshino,[2] Kentaro Uesugi,[2] Naoto Yagi,[2] Barbara K. Pierscionek,[3] and Usha P. Andley[4]

[1]Beijing Advanced Innovation Centre for Biomedical Engineering, School of Engineering Medicine, Beihang University, Beijing, China
[2]Japan Synchrotron Radiation Research Institute (SPring8), Sayo, Hyogo, Japan
[3]Faculty of Health, Education, Medicine and Social Care, Medical Technology Research Centre, Anglia Ruskin University, Bishops Hall Lane, Chelmsford, United Kingdom
[4]Department of Ophthalmology and Visual Sciences, Washington University School of Medicine, St. Louis, MO, United States

Correspondence: Barbara K. Pierscionek, Faculty of Health, Education, Medicine and Social Care, Medical Technology Research Centre, Anglia Ruskin University, Bishops Hall Lane, Chelmsford CM1 1SQ, UK; barbara.pierscionek@aru.ac.uk. Usha Andley, Department of Ophthalmology and Visual Sciences, Washington University School of Medicine, St. Louis, MO, USA; andley@wustl.edu.

Received: January 5, 2022
Accepted: April 22, 2022
Published: May 16, 2022

Citation: Wang K, Hoshino M, Uesugi K, Yagi N, Pierscionek BK, Andley UP. Oxysterol compounds in mouse mutant αA- and αB-crystallin lenses can improve the optical properties of the lens. *Invest Ophthalmol Vis Sci.* 2022;63(5):15. https://doi.org/10.1167/iovs.63.5.15

Purpose. To investigate how cataract-linked mutations affect the gradient refractive index (GRIN) and lens opacification in mouse lenses and whether there is any effect on the optics of the lens from treatment with an oxysterol compound.

Methods. A total of 35 mice including wild-type and knock-in mutants (*Cryaa*-R49C and *Cryab*-R120G) were used in these experiments: 26 mice were treated with topical VP1-001, an oxysterol, in one eye and vehicle in the other, and nine mice were untreated controls. Slit lamp biomicroscopy was used to analyze the lens in live animals and to provide apparent cataract grades. Refractive index in the lenses of 64 unfixed whole mouse eyes was calculated from measurements with X-ray phase tomography based on X-ray Talbot interferometry with a synchrotron radiation source.

Results. Heterozygous *Cryaa*-R49C lenses had slightly irregularly shaped contours in the center of the GRIN and distinct disturbances of the gradient index at the anterior and posterior poles. Contours near the lens surface were denser in homozygous *Cryab*-R120G lenses. Treatment with topical VP1-001, an oxysterol, showed an improvement in refractive index profiles in 61% of lenses and this was supported by a reduction in apparent lens opacity grade by 1.0 in 46% of live mice.

Conclusions. These results indicate that α-crystallin mutations alter the refractive index gradient of mouse lenses in distinct ways and suggest that topical treatment with VP1-001 may improve lens transparency and refractive index contours in some lenses with mutations.

Keywords: refractive index, X-ray, alpha crystallin mutant lenses, oxysterol

The crystallin family of proteins is essential for lens transparency, and altered short-range interactions of crystallins are thought to be responsible for cataract-associated light scattering.[1] Distributions and classes of crystallin proteins in the lens have been linked to the gradient of refractive index (GRIN) profile and refractive index magnitude.[2] A high concentration of crystallin proteins provides transparency and creates the unique GRIN profile within the lens that is needed to provide the high level of image quality required for vision.[1] Because the lens has limited capacity for new protein synthesis, crystallins must remain soluble and stable for decades[1], a remarkable feature facilitated in part by the chaperone α-crystallin, which helps maintain protein stability and preserve lens transparency.[3,4] It has been shown that α-crystallin accounts for nearly 50% of the protein mass in human lenses and is known to interact with non-native proteins to prevent their irreversible aggregation and insolubilization in vitro.[5] In mammalian lenses, αA- and αB-crystallin are present as dynamic hetero-oligomers in a 3:1 ratio. The active form of αB-crystallin consists of dimers and larger oligomers[4] that prevent substrate proteins from aggregating via numerous non-specific and low-affinity amphipathic interactions.[6,7] Mutations or post-translational modifications leading to structural or functional alterations in αA- or αB-crystallin (*Cryaa* and *Cryab*) are associated with aggregation[8] and early-onset hereditary cataracts[9–11]; mutants *Cryaa*-R49C and *Cryab*-R120G are associated with aggregation in vitro and early-onset cataracts in humans.[9,12–14] The R120G mutation, which occurs at a conserved position of αB-crystallin, alters the aggregation behavior of the protein by disrupting its two native salt bridges, which normally contribute to the dimerization of two αB-crystallin protomers across an antiparallel β-sheet interface.[4] Repeating units of αB-crystallin dimers typically assemble into larger oligomers, but R120G disrupts the overall assembly and function of the chaperone.[4] We

previously showed that the lenses of *Cryab*-R120G knock-in mice contain a greater proportion of insoluble, aggregated αB-crystallin and develop opacities at an early age compared with wild-type (WT) mice.[15] In addition, *Cryab*-R120G oligomers in solution had a two- to threefold higher average molecular mass than WT αB-crystallin. Similar to *Cryab*-R120G, *Cryaa*-R49C knock-in mice develop lens opacity at an early age and exhibit a smaller proportion of water-soluble αA-crystallin compared with WT mice.[13] Importantly, these mutations impair the chaperone functions of crystallins.[14,16] Interactions with client proteins, such as vimentin, are increased for *Cryab*-R120G compared with WT crystallins in epithelial and fiber cells of mouse lenses.[15] Thus, in addition to aging of the lens, *Cryab*-R120G can promote aggregate formation that leads to lens opacification and cataract.[15,17,18]

Several mutations in crystallin genes have been shown to lead to opacification in human lenses and contribute to crystallin aggregation and insolubilization.[13–15,19] Given that these mutations cause cataract, there are likely to be alterations in the refractive index profile of mutant lenses compared with those of WT lenses.[20]

Numerous techniques can be used to measure the GRIN of eye lenses, including those that require tissue slicing[21,22] to more noninvasive approaches, such as ray tracing[23,24] and fiberoptic sensing.[25,26] Refractive index has also been estimated from free water detected magnetic resonance imaging,[27–29] but this does not consider protein-bound water, which also contributes to refractive index, nor the fact that proportions of free and bound water change with age.[30] Ideally, refractive index should be measured on whole lenses in any given plane and with a level of accuracy that can detect physiologically relevant fluctuations or irregularities. Conventional X-ray microtomography can quantify sample density but does not distinguish soft tissue structures within the eye. X-ray phase tomography, based on X-ray Talbot interferometry, using a synchrotron radiation source is a recent advancement that allows such measurements to be obtained from intact lenses in any plane[31] and has yielded the most detailed three-dimensional GRIN profiles to date.[32,33] The technique can be used to measure the GRIN and can also detect any disturbances to its form in cataractous lenses because X-rays, unlike visible light, can penetrate opacities.[34] The X-ray Talbot grating interferometer, which takes advantage of Moiré fringes generated by phase and absorbance gratings, is superior to other X-ray interferometers, such as the Bonse-Hart instrument, in simplicity of its configuration and in the robustness of phase measurement. This makes it ideal for investigating refractive index and protein density distributions across the murine lens.[35] Measurements obtained using this method in the human lens suggest that the refractive index gradient is not smooth but rather exhibits distinct irregularities and fluctuations[32,33]: characteristics that have been suggested from an earlier study of African cichlid fish lenses.[36]

The aim of the study was to investigate whether X-ray phase tomography could distinguish subtle changes in GRIN profiles, in mutant mouse lenses, that were not found previously using other methods and whether this technique could also detect the effects of an oxysterol that had been reported to restore transparency in cataractous lenses.[37] Our results indicate that minor discontinuities or fluctuations in the index profile, which may have biological significance, can be reliably detected using this method. Improvements in the optics of the lens as evidenced from measurements of the GRIN profile and supported by results from slit-lamp images, were seen in some lenses that had been treated with oxysterol compared to lenses from the same mouse that had not received this treatment.

Methods

Animals

Experiments were conducted on C57BL/6J mice, a strain with mutations that cause cataract development: a knock-in mutation of αB-crystallin (*Cryab*-R120G) or of αA-crystallin (*Cryaa*-R49C).[12,13] All animal procedures adhered to the ARVO Statement for Use of Animals in Ophthalmic and Vision Research. All animal procedures were approved by the Institutional Animal Care and Use Committee at Washington University in St. Louis (St. Louis, MO, USA). The Mouse Genetics Core at Washington University was responsible for housing, care, breeding, and genotyping of mice. Single nucleotide polymorphism services from DartMouse (Dartmouth Geisel School of Medicine, Lebanon, NY, USA) previously converted these mice to a C57BL/6J background using speed congenics.[38] These mice do not carry the CP49 mutation; thus cataracts in these mice are unlikely to be due to the CP49 mutation present in the 129Sv strain.

Treatment With VP1-001

A total of 35 mice (12 male and 23 female mice, 6 to 24 months old) were used for these studies: 26 mice were treated with vehicle (8% cyclodextrin) in the left eye and 2 mM VP1-001, also known as compound 29 and 25-hydroxycholesterol,[37,39] (in 8% cyclodextrin) in the right eye each administered as a single drop onto the ocular surface, three times per week for two weeks for a total of seven treatments.[39] The vehicle used for this study was prepared in sterile phosphate buffered saline solution. An additional nine mice were untreated (i.e., no vehicle or VP1-001 administration) for separate control experiments. WT (C57BL/6J) (255–738 days old, 13 mice), heterozygous *Cryab*-R120G (402 days old, three mice), homozygous *Cryab*-R120G (185–260 days old, 13 mice), and heterozygous *Cryaa*-R49C (186–416 days old, six mice) mice were used (Supplementary Files, Supplementary Table S1). Homozygous *Cryaa*-R49C mice develop severe cataracts and small eyes at birth[9] and were not investigated in this study. The heterozygous *Cryaa*-R49C mice develop lens opacities with no other ocular phenotype; 20% of the *Cryab*-R120G-Het and *Cryab*-R120G-Hom mice have a small eye and lens, and 5% of *Cryab*-R120G-Het mice and 16% of *Cryab*-R120G-Hom mice develop corneal abnormalities.[15] No samples used in this study had a corneal opacity or reduced eye or lens size. The knock-in mice we investigated start to develop cataracts at approximately three weeks of age, and these become progressively worse as the animal ages.[15,40] Thus these mice serve as a reliable model for human age-related cataracts that take decades to develop and may provide a better understanding of cataracts in families who are heterozygous for the autosomal dominant mutations *Cryaa*-R49C or *Cryab*-R120G.[41,42]

Slit Lamp Biomicroscopy

Nonanesthetized mice were analyzed by slit lamp biomicroscopy using a Topcon instrument (model BG-2GN, serial

number 941752; Topcon, Oakland, NJ, USA).[39] Pupils were dilated before lens examination using 1% USP tropicamide ophthalmic solution and 10% USP phenylephrine hydrochloride solution.[39] The slit length was 14 mm and slit width was between 1 and 2 mm; these settings were kept constant for all eyes examined. Images were captured at magnification ×40, and the slit was placed orthogonal to the mouse eye for optimal viewing of the lens.[39] Apparent cataract grades were determined in the vehicle- and VP1-001–treated eyes. After slit lamp analysis, mice were euthanized by CO_2 inhalation consistent with the 2013 AVMA guidelines. Unfixed whole eyes in minimum essential medium with penicillin and streptomycin antibiotics collected from WT, *Cryab*-R120G, and *Cryaa*-R49C mice were shipped to Japan (SPring-8) for X-ray phase tomographic analysis.

X-Ray Phase Tomography Using X-Ray Talbot Grating Interferometer

Optical parameters of the ocular samples were analyzed using X-ray phase tomography based on the X-ray Talbot interferometry at beamline BL20B2 in SPring-8.[32–35,43] The X-ray beam was fine-tuned to 25 keV by a Si(111) double-crystal monochromator and passed through two transmission gratings, phase grating (G1) made of Ni and absorption grating (G2) made of Au, with respective pattern thicknesses of 4.35 µm and 110 µm, a pitch of 4.8 µm, and a pattern size area of 50 × 50 mm^2. Moiré fringe patterns generated by passage of the X-ray beam through the sample, G1, and G2 were detected by a visible-light conversion type X-ray imaging detector. Final visible-light images were detected by a scientific CMOS camera (ORCA Flash 4.0; Hamamatsu Photonics, Hamamatsu, Japan). The effective pixel size was 12.7 µm or 15.4 µm. Samples were fixed on a rotator for the collection of 900 projection images per sample, during which G2 was shifted relative to G1 with a Piezo stage for phase retrieval using a five-step fringe-scan method. Final phase images were generated by integration of the differential phase images. The total measurement time for each lens was 50 minutes. In the tomographic reconstruction, a filtered back projection method was used.

Calculating Refractive Index

Protein concentrations of the samples were determined using phase shift values obtained from the tomographic reconstruction.[32,44] The experimentally obtained phase shift values were calibrated with standards of known density. A refractive increment applicable to proteins (0.18 mL/g) was used to calculate the refractive index of each lens, which positively correlates to protein concentration.[32,43,44]

Data Analysis

MatLab version 2020a (Natick, MA, USA) was used for post-processing data analysis, while a custom-developed code that reconstructs X-ray phase tomographic three-dimensional data was used to generate two-dimensional contour and three-dimensional mesh images of the mid cross-sectional planes in the sagittal direction of all measured murine lenses. An increment of 0.01 in refractive index was selected to distinguish between contours.

Results

Structural Characteristics of WT and Crystallin Mutant Mouse Lenses

The lenses of in vivo mice were examined by slit lamp biomicroscopy from which gradings of cataracts were made as shown in Figure 1. These gradings were not quantified by densitometric analysis and hence are apparent gradings. Three WT lenses of different ages: 255 days, 493 days, and 738 days have different degrees of opacification, with the highest opacity grading of 4 found in the 493-day-old lens. This WT lens is compared to three sets of mutant lenses that were closest in age to this WT lens. The *Cryaa*-R49C lenses, which were 416 days of age, had lower apparent cataract grades, of 2.5 and 3.5, compared to those for the 493-day-old WT lens (Fig. 1). The *Cryab*-R120G-Het lenses, aged 402 days had slightly lower apparent cataract gradings (both had an apparent grading of 3.5) compared to the WT lens (Fig. 1) whereas the *Cryab*-R120G-Hom lenses, aged 449 days, were both almost opaque and had apparent cataract gradings of 4 (Fig. 1). It should be noted that although slit lamp settings were constant for all measurements, illumination appears brighter where there is greater opacification because this causes a greater degree of light scatter in such lenses compared to lenses that are more transparent.

The GRIN profiles of WT, *Cryaa*-R49C, and *Cryab*-R120G lenses from whole eyes are seen on Figures 2 to 5. The WT lenses in Figure 2 show relatively smooth contours and three-dimensional GRIN profiles for the 255-day-old lens (Figs. 2a, 2d). Central contours are regular in the lens aged 493 days but there are irregularities in the outer contours in the anterior (a) and posterior (p) polar regions (as indicated by the red arrows). This indicates a localized steepening of the GRIN and therefore a higher protein density in that region (Figs. 2b, 2e). This would cause disturbance in the refraction of light leading to increase in light scatter and would explain the high grade of opacification seen in the slit lamp image of this lens (Fig. 1). The oldest lens also has irregular peripheral contours, particularly in the anterior polar region (as indicated by the red arrow in Fig. 2c) and a compacting of the contours that could indicate a slight steepening of the GRIN profile in this region. The lower apparent grade of cataract in this lens compared to the 493-day-old lens (Fig. 1) may be because the disturbances to the GRIN profile are more localized and, hence, the light scatter is less diffuse than in the 493-day-old lens. There is also a widening of the nuclear, peak refractive index region, with age, as seen in Figure 2; the diameter of the innermost contour increases from 0.63 mm at 255 days old to 0.82 mm at 738 days old).

The three-dimensional GRIN profiles and refractive index contours show that *Cryaa*-R49C heterozygous (Het) lenses had slightly more irregularly shaped contours in the center and noticeably greater disturbances of peripheral contours in the polar regions (Figs. 3b, 3e and 3c, 3f) compared to the WT lens (Figs. 3a, 3d). The apparent cataract grades for these lenses were 2.5, and 3.5, respectively (Fig. 1). Although the WT lens had a higher grading, the *Cryaa*-R49C-Het lenses had more discrete localized opacities that are manifested in greater disturbances in the refractive index

Investigative Ophthalmology & Visual Science

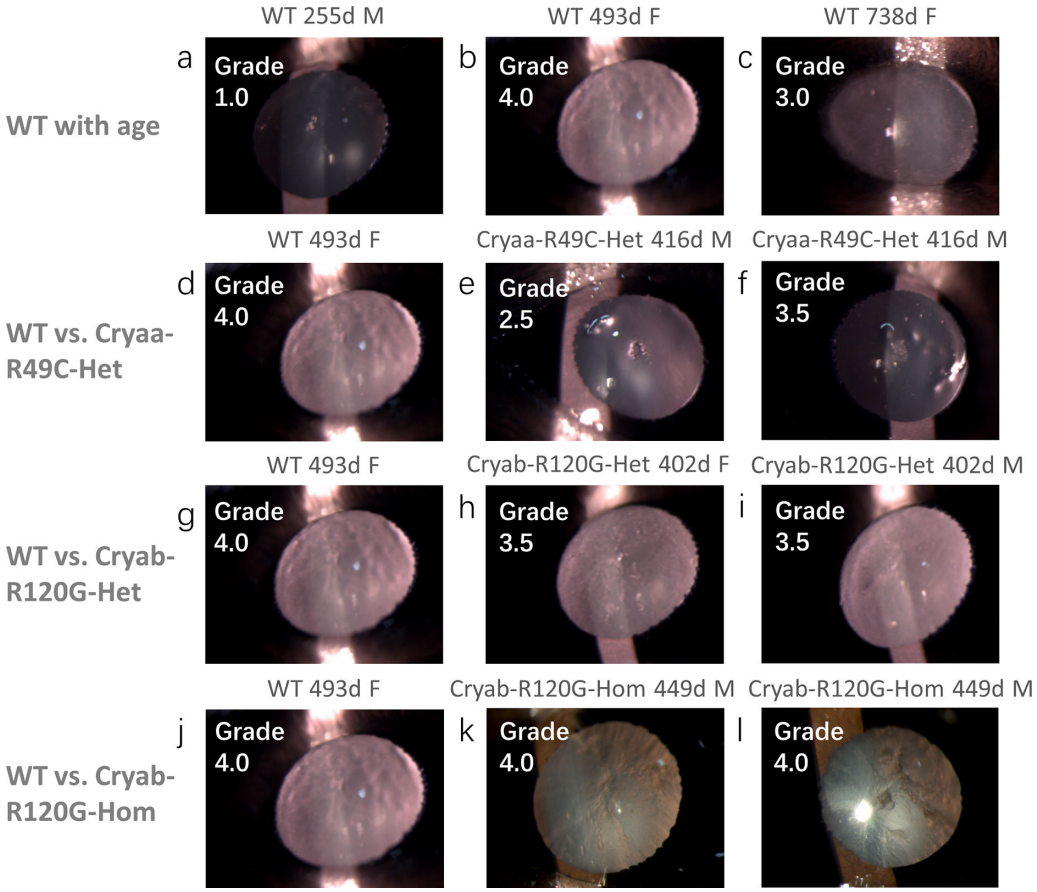

Figure 1. Slit lamp images of eyes from mice of different genotypes. Representative slit lamp images show the extent of lens opacity in WT lenses aged (**a**) 255 days, (**b**) 493 days, and (**c**) 738 days with apparent cataract gradings of 1.0, 4.0, and 3.0, respectively. The 493-day-old WT lens is compared in **d** with 416-day-old *Cryaa*-R49C-Het lenses (**e** and **f**); both had lower apparent cataract gradings than the WT 493-day-old lens. The 493-day-old WT lens is compared in **g** with 402-day-old *Cryab*-R120G-Het lenses (**h** and **i**) and in **j** with 449-day-old *Cryab*-R120G-Hom lenses (**k** and **l**). The apparent cataract gradings for the *Cryab*-R120G-Het lenses were lower than in the WT lens; the *Cryab*-R120G-Hom lenses were very opacified and had the same apparent grading as the WT lens. Images shown are of OS (**a, b, d, g, h, i, k, j**) and OD (**c, e, f, l**) lenses. The nasal side is on the left side of the image in OS lenses and on the right side of the image in OD lenses.

profiles. There are few notable distinctions between the GRIN profiles and refractive index contours in the *Cryab*-R120G-Het lenses (Figs. 4b, 4e and 4c, 4f) compared to those of the WT lens (Figs. 4a, 4d) with only slightly greater disturbances of refractive index in the peripheral regions of the mutant lenses (as indicated by arrows) in Figs. 4b and c. The apparent cataract grading was slightly higher for the WT (grade 4.0) than for the mutant lenses (grade 3.5) as seen in Figure 1.

Although the apparent cataract grading of the slit lamp images was the same in the 493-day-old WT lens and the 449-day-old *Cryab*-R120G-Hom lenses (Fig. 1), the latter were more opaque. The significant light scatter in the WT lens appeared to be from the periphery of the lens; the opacification in the mutant lenses was from deeper layers. This is seen in the contour plots and three-dimensional GRIN profiles in Figure 5. The mutant lenses have very distorted and narrow contour plots that are not concentric but skewed and misshapen with localized disturbances in the refractive index indicative of protein aggregates (indicated by arrows in Figs. 5b, 5e and 5c, 5f). The three-dimensional profiles show the narrowing of the refractive index profile clearly as steep forms with sharp ridges on the surface (indicated by arrows in Figs. 5e and 5f).

Effects of VP1-001 Treatment on Refractive Index and Transparency

The effect of VP1-001 treatment on transparency of the lens is seen in Figure 6, which shows slit lamp images of lenses after treatment contralaterally with either vehicle or VP1-001. The pairs shown include a WT lens aged 270 days, (A), *Cryaa*-R49C-Het lens aged 186 days (B), *Cryab*-R120G-Het aged 402 days (C), and *Cryab*-R120G-Hom mouse lenses aged 185 days (D). In all pairs there was a greater level of transparency in the VP1-001-treated lens. The comparatively high level of brightness seen in the *Cryab*-R120G-Hom OS, vehicle treated lens, is likely to result from significant light scatter that is seen when light is projected to regions of refractive index fluctuation. Some of the lens images appear slightly reduced in size and this could be because the position of the mouse eye may have moved slightly during the measurement. Apparent cataract grades of all treated mice are shown in the Table and are higher in all vehicle treated lenses compared to their respective VP1-001–treated counterparts.

Nine additional mice (WT n = 5, *Cryaa*-R49C-Het n = 2, and *Cryab*-R120G-Hom n = 2) with no VP1-001 or vehicle treatment were subjected to slit-lamp analysis with results

Investigative Ophthalmology & Visual Science

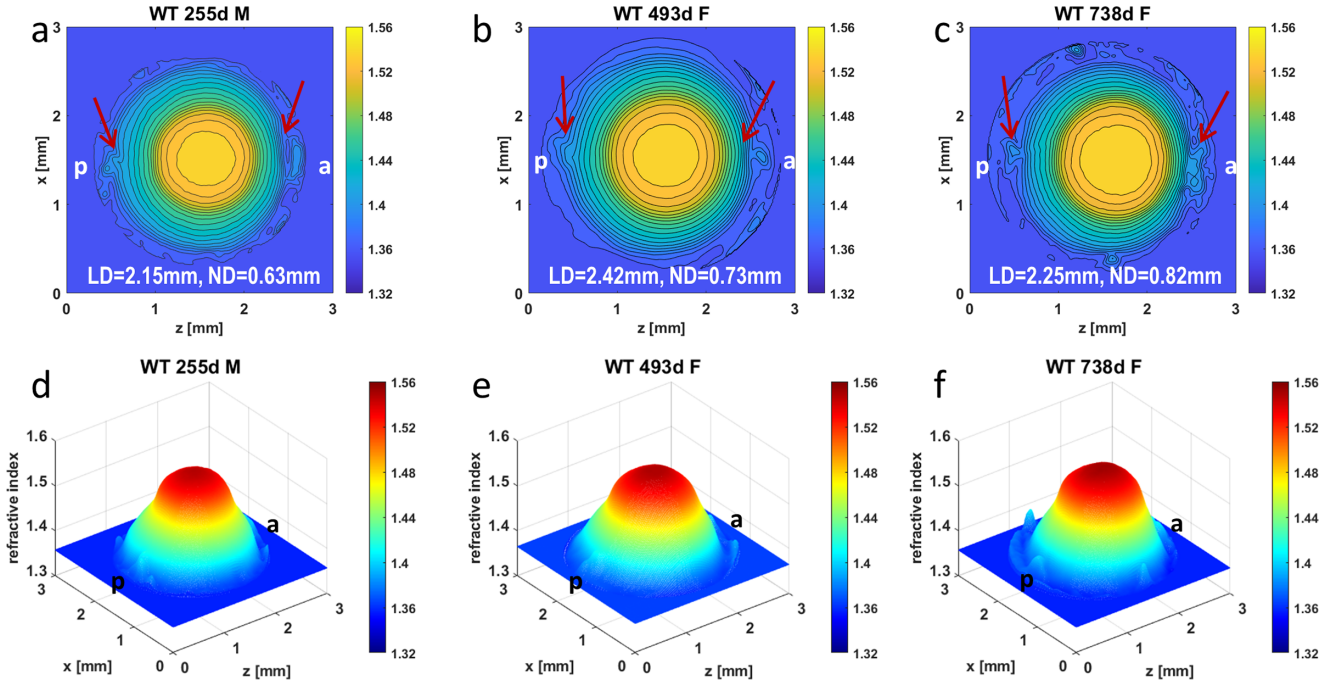

Figure 2. Comparison of refractive index profiles in WT lenses with age. Refractive index distributions in the mid-sagittal cross-sectional plane of each WT mouse lens shown both as contour plots (*first row*) and as three-dimensional GRIN profiles (*second row*) for lenses aged 255 days (**a, d**) [ID 1378-3 Supplementary Table S1], 493 days (**b**, **e**) [ID 1078-4 Supplementary Table S1] and 738 days (**c, f**) [ID 1170-5 Supplementary Table S1]. Magnitudes of refractive index are indicated using color bar on the right side of each image. Slight disturbances at the poles of the 255-day-old WT lens, shown by *arrows* (**a**) are likely to be capsular damage. The *arrows* in **b** show irregularities in peripheral contours in the polar regions of the 493-day-old lens; the *arrows* in **c** show perturbed contours near the anterior pole with slighter perturbation at the posterior pole. The maximum refractive index found in the innermost contour is 1.54; adjacent contours differ in refractive index by a value of 0.01. WT = wild type, d = day, F = female, M = male, a = anterior pole, p=posterior pole, LD = lens diameter, ND = diameter of the innermost contour.

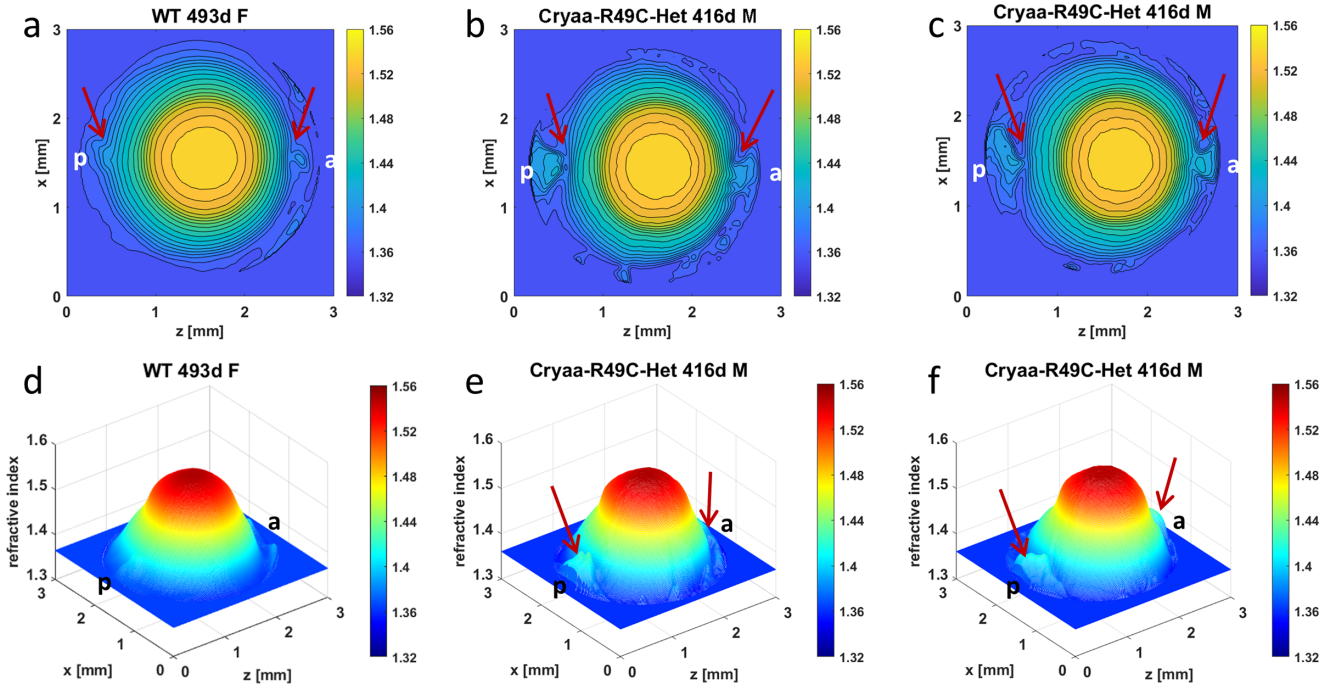

Figure 3. Comparison of refractive index profiles between WT lens and *Cryaa*-R49C-Het lenses. Refractive index distributions in the mid-sagittal cross-sectional plane of each mouse lens shown both as contour plots (*first row*) and as 3-dimensional GRIN profiles (*second row*) for a 493-day-old WT lens (**a, d**) [ID 1078-4 Supplementary Table S1], and two 416-day-old *Cryaa*-R49C-Het lenses (**b, e** [ID 1310-2 Supplementary Table S1] and (**c, f**) [ID 1311-5 Supplementary Table S1]. Magnitudes of refractive index are indicated by the color bar on the right side of each image. Slight disturbances, shown by *arrows*, are seen at the poles of the WT lens (a) and could be a manifestation of age-related changes. *Arrows* in **b** and **c** indicate significant disturbances in the refractive index gradient in the polar regions. WT = wild type, d = day, F = female, M = male, a = anterior pole, p = posterior pole.

Investigative Ophthalmology & Visual Science

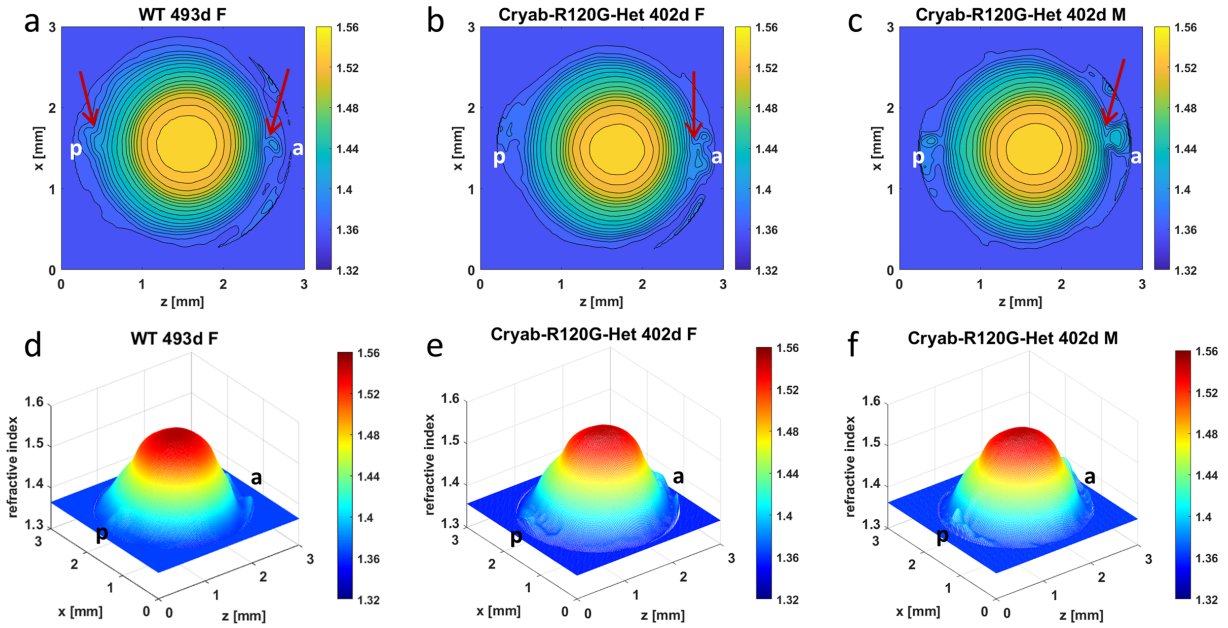

Figure 4. Comparison of refractive index profiles between WT lens and *Cryab*-R120G-Het lenses. Refractive index distributions in the mid-sagittal cross-sectional plane of each mouse lens shown both as contour plots (first row) and as three-dimensional GRIN profiles (second row) for a 493-day-old WT lens (**a, d**) [ID 1078-4 Supplementary Table S1], and two 402-day-old *Cryab*-R120G-Het lenses (**b, e**) [ID 1145-1 Supplementary Table S1], and (**c, f**) [ID 1144-6 Supplementary Table S1]. Magnitudes of refractive index are indicated using color bar on the right side of each image. Slight disturbances, shown by *arrows*, are seen at the poles of the WT lens (a) and could be a manifestation of age-related changes. *Arrows* in **b** and **c** indicate greater disturbances of refractive index gradient in the anterior polar regions than seen in the WT lens (**a**). This is particularly evident in **c**. WT = wild type, d = day, F = female, M = male, a = anterior pole, p = posterior pole.

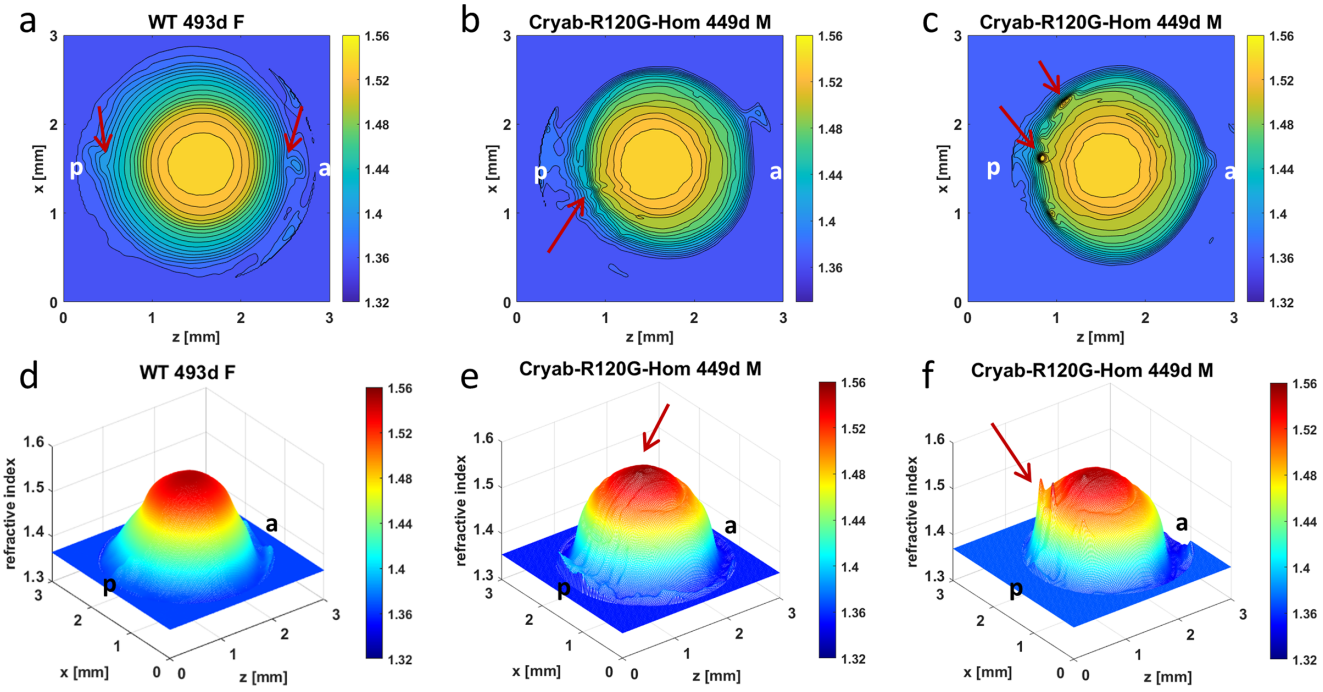

Figure 5. Comparison of refractive index profiles between WT lens and *Cryab*-R120G-Hom lenses. Refractive index distributions in the mid-sagittal cross-sectional plane of each mouse lens shown both as contour plots (*first row*) and as three-dimensional GRIN profiles (second row) for a 493-day-old WT lens (**a, d**) [ID 1078-4 Supplementary Table S1], and two 449-day-old *Cryab*-R120G-Hom lenses (**b, e**) [ID 905-3 Supplementary Table S1] and (**c, f**) [ID 906-8 Supplementary Table S1]. Magnitudes of refractive index are indicated using color bar on the right side of each image. Slight disturbances, shown by arrows, are seen at the poles of the WT lens (**a**) and could be a manifestation of age-related changes. The refractive index contours in the old *Cryab*-R120G-Hom lenses are narrow, not concentric and misshapen (**b** and **c**). *Arrows* show disturbances in refractive index indicative of localized high protein concentration (**b,e** and **c,f**). The three-dimensional profiles (**e** and **f**) are narrow and steep with ridges (shown by *arrows*) on the surface. WT = wild type, d = day, F = female, M = male, a = anterior pole, p = posterior pole.

Investigative Ophthalmology & Visual Science

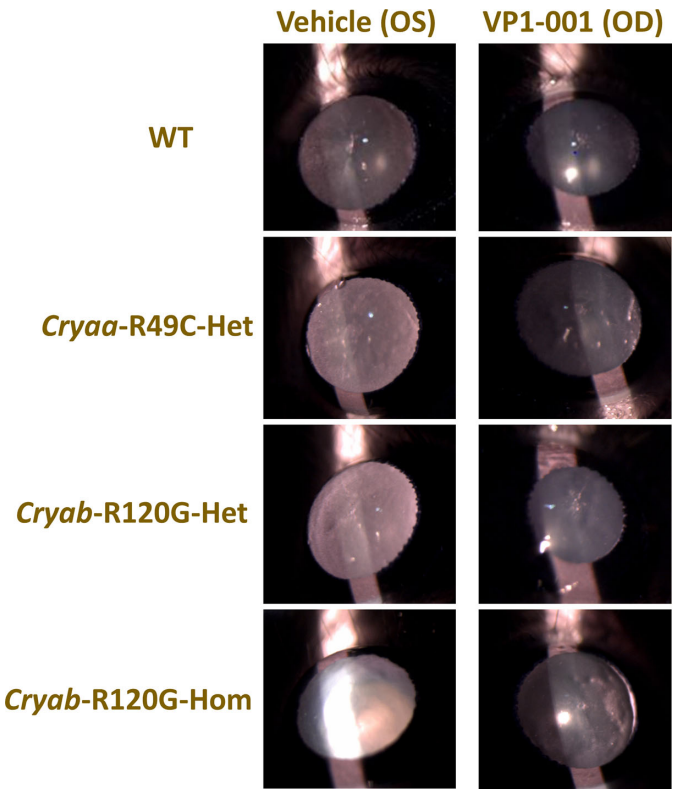

Figure 6. Slit lamp images of eyes from mice of different genotypes. Representative slit lamp images show the comparison between vehicle-treated (left) lenses and VP1-001-treated (right) lenses in (**A**) WT lens pair aged 270 days, (**B**) *Cryaa*-R49C-Het lens pair aged 186 days, (**C**) *Cryab*-R120G-Het lens pair aged 402 days, and (**D**) *Cryab*-R120G-Hom lens pair aged 185 days. (The nasal side is on the left side of the image in OS [vehicle] lenses and on the right side of the image in OD [VP1-001] lenses).

shown in Supplementary Table S2. Data for these untreated mice were included to ascertain if there were any effects of eye drop treatment on apparent cataract grade or refractive index profiles. A comparison between refractive index profiles from WT mice of comparatively matched ages that had been treated with either vehicle or VP1-001 (Figs. 7b and 7d) and those that had not been treated (controls) (Figs. 7a and 7c) is shown in Figure 7. The control lens pair in Figure 7a had a relatively low apparent grading of opacification (Supplementary Table S2), and yet there are disruptions seen in the peripheral regions that are likely to be indicative of capsular damage that occurred after the slit-lamp images were taken. The other control pair (Fig. 7c) also had a moderately low grading (Supplementary Table S2) and smooth GRIN contours and three-dimensional profiles with a slight disturbance at the anterior pole in the OD WT lens (as marked by the arrow in Fig. 7c). Marked differences are seen in the two treated pairs of lenses (Figs. 7b and 7d), in both pairs the vehicle-treated lenses have disturbances in the refractive index form (as noted by arrows) whilst the corresponding VP1-001 lenses have regularly spaced, undisturbed contours and smooth 3-dimensional profiles. This concurs with the apparent gradings of opacification seen in the Table which show higher grading in the vehicle treated compared to the VP1-001–treated lenses.

All four *Cryaa*-R49C-Het mice showed an improvement in apparent cataract grade by at least grade 1.0 after VP1-001 treatment (mean apparent cataract grade vehicle vs. VP1-001 was 3.1 vs. 1.1) (Table). Differences are also found in the refractive index profiles (Fig. 8). The disturbances in the refractive index contours and in the three-dimensional plots seen in the anterior pole of the vehicle treated *Cryaa*-R49C-Het lens are slightly reduced in its VP1-001–treated counterpart (Fig. 8a). Similar results are demonstrated for the *Cryab*-R120G lenses (Fig. 8b). All three *Cryab*-R120G-Het mouse lenses showed a decrease in apparent cataract grade of 1.0 or more with VP1-001 treatment (mean apparent cataract grade vehicle vs.VP1-001 was 3.5 vs. 2.0) (Table).

Three of the 11 *Cryab*-R120G-Hom mice (27%) exhibited lower apparent cataract grades with VP1-001 treatment (Table). Results vary when considering the GRIN profiles (Fig. 9). Lenses that do not manifest changes in GRIN profiles between VP1-001 treatment and treatment with vehicle are shown in Figures 9a, 9c, and 9e, whereas lenses that demonstrate significantly improved GRIN profiles and contour plots after treatment with VP1-001 compared to their partner lenses treated with vehicle are shown in Figures 9b, 9d, 9f. This is most evident in Figure 9b where the GRIN profile in the vehicle treated lens is smaller with a sharper peak and refractive index contours are less regular than seen in its partner VP1-001–treated lens. More subtle changes are seen in the lens pair in Figure 9d with more irregular spreading of contours (as indicated by the arrows in the vehicle-treated lens) than in the VP1-001 lens. In Figure 9f, there is a noticeable difference between the lens pair: the vehicle treated lens shows localized spots of high refractive index, evident in the 3-dimensional GRIN profile and in the contour plots; this is not seen in the lens treated with VP1-001. Overall, 61% of the 26 mice of all genotypes treated with VP1-001 in one eye showed an improvement in the refractive index profiles.

Investigative Ophthalmology & Visual Science

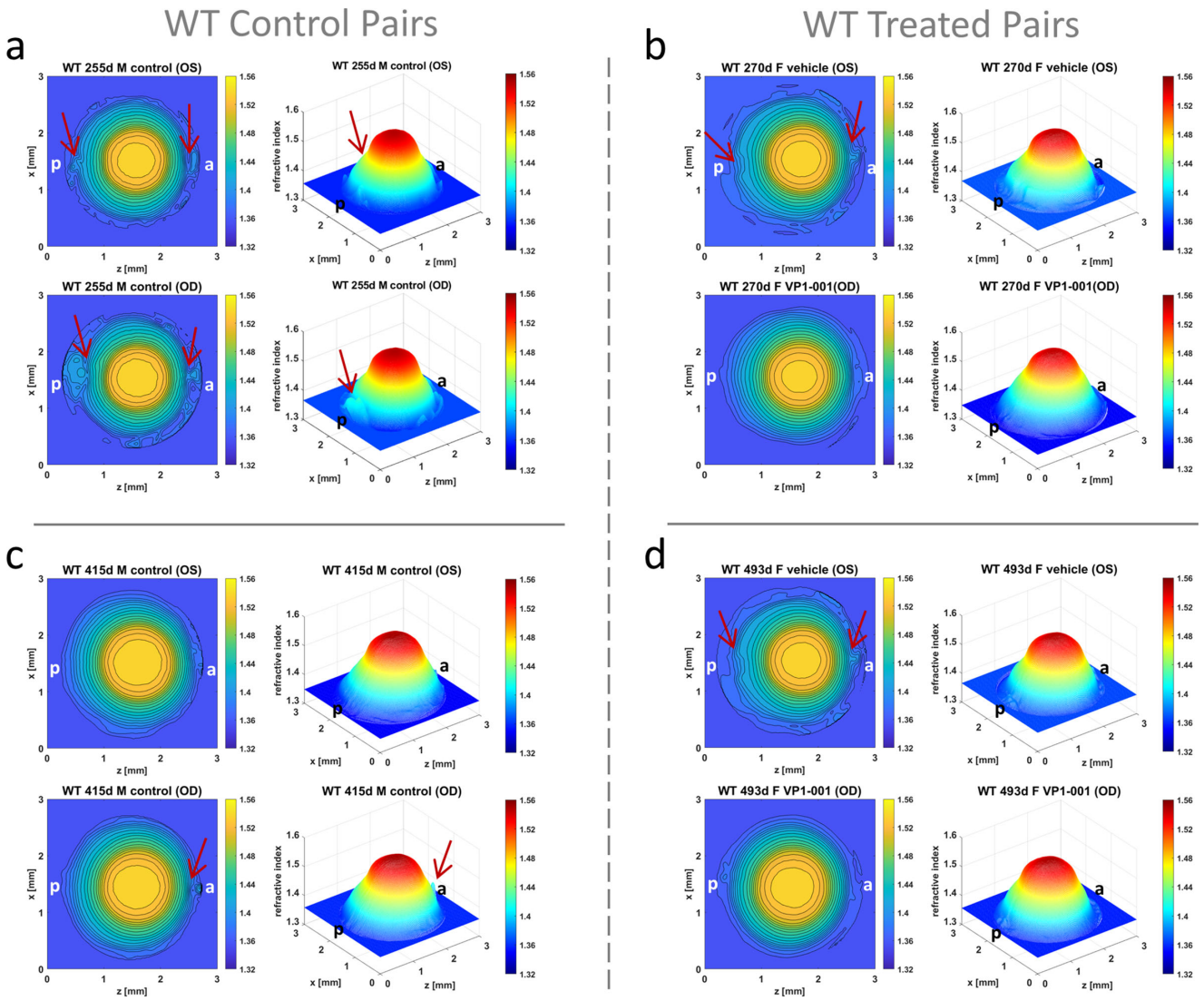

Figure 7. Comparison of refractive index profiles between control and treated eyes of similar ages. Refractive index distributions shown as contour plots in the mid-sagittal cross-sectional plane and as three-dimensional GRIN profiles in control lenses from mice that had not been treated with either vehicle or VP1-001 aged (**a**) 255 days [ID 1378-3 Supplementary Table S1] and (**c**) 415 days [ID 938-1 Supplementary Table S1] and in lenses from mice treated with vehicle in the OS eye and with VP1-001 in the OD eye aged (**b**) 270 days [ID 1210-3 Supplementary Table S1] and (**d**) 493 days [ID 1077-3 Supplementary Table S1]. The contour plots and three-dimensional profiles are generally indicative of normal optical function with show slight disturbances (marked by *arrows*) in the polar regions of the 255-day-old WT lens (**a**) that could be a manifestation of capsular damage. There is a slight disturbance to the refractive index in the anterior pole of the 415-day-old OD lens as marked by the arrows in the contour plot and the three-dimensional profile (**c**). The treated pairs **b** and **d** show some small irregularities in the polar regions (marked by *arrows* on the contour plots) in the vehicle treated lenses; these irregularities are not apparent in the lenses treated with VP1-001 (**b** and **d**). a = anterior pole, p = posterior pole.

Discussion

Age-related damage or mutations of the lens chaperone proteins αA- and αB-crystallin lead to their destabilization and aggregation, which culminate in cataract formation. The *Cryab*-R120G mutation is associated with human lens cataracts and myopathy in juveniles, and the *Cryaa*-R49C mutation is linked with early-onset human hereditary cataracts. Using knock-in mice that express *Cryab*-R120G or *Cryaa*-R49C mutations associated with human cataracts, we previously analyzed the in vivo substrates of these molecular chaperones in the lens by proteomics, examined the transcriptome changes in lenses associated with cataract development, and developed strategies to reduce lens opacification using small molecules in vivo.[6,37,45,46] However, before the current study, the effects of α-crystallin mutations on refractive index gradients in lenses have not been compared with those in WT lenses. Our previous work showed that VP1-001 treatment of mouse eyes in vivo reduces lens opacity grade and increases the proportion of soluble protein in the mouse lenses.[37,39] The effect of VP1-001 treatment on refractive index measurement by X-ray phase tomography has not previously been investigated. The refractive index contours revealed by this method provide additional information beyond that provided by slit lamp biomicroscopy, allow more detailed visualization of areas affected by *Cryaa* and *Cryab* mutations and indicate, for the first time, potential mechanisms by which VP1-001 may improve the optics

Investigative Ophthalmology & Visual Science

Table. Apparent Cataract Grades of Mice of Different Genotypes and Ages Used for *In Vivo* Eye Drop Administration With Vehicle or VP1-001

Genotype	Mouse ID	Age (Days)	Gender	Apparent Cataract Grade	
				OS (Vehicle)	OD (VP1-001)
WT					
	1209-7	269	M	3	1.5
	1210-3	270	F	3	1
	1211-4	270	F	2	0
	1076-1	493	F	2.5	1
	1077-3	493	F	3	1.5
	1078-4	493	F	3	1
	1079-6	493	F	2.5	0.5
	1080-7	493	F	3.5	2
Cryaa-R49C-Het					
	1235-2	186	F	3.5	1.5
	1236-4	186	F	2.5	0.5
	1237-7	186	F	3.5	1.5
	1238-1	186	M	3	1
Cryab-R120G-Het					
	1144-6	402	M	3.5	2.5
	1145-1	402	F	3.5	1.5
	1146-3	402	F	3.5	2
Cryab-R120G-Hom					
	1226-5	185	F	2.5	2
	1231-4	185	F	4	2
	1233-3	185	M	3	2.5
	1212-1	260	F	4	3.5
	1213-3	260	F	3.5	2.5
	1214-5	260	F	3.5	2.5
	1215-2	260	M	3	2
	1216-4	260	M	3.5	3
	1219-4	262	F	3.5	3
	1204-2	323	F	4	3.5
	1150-4	380	F	4	3

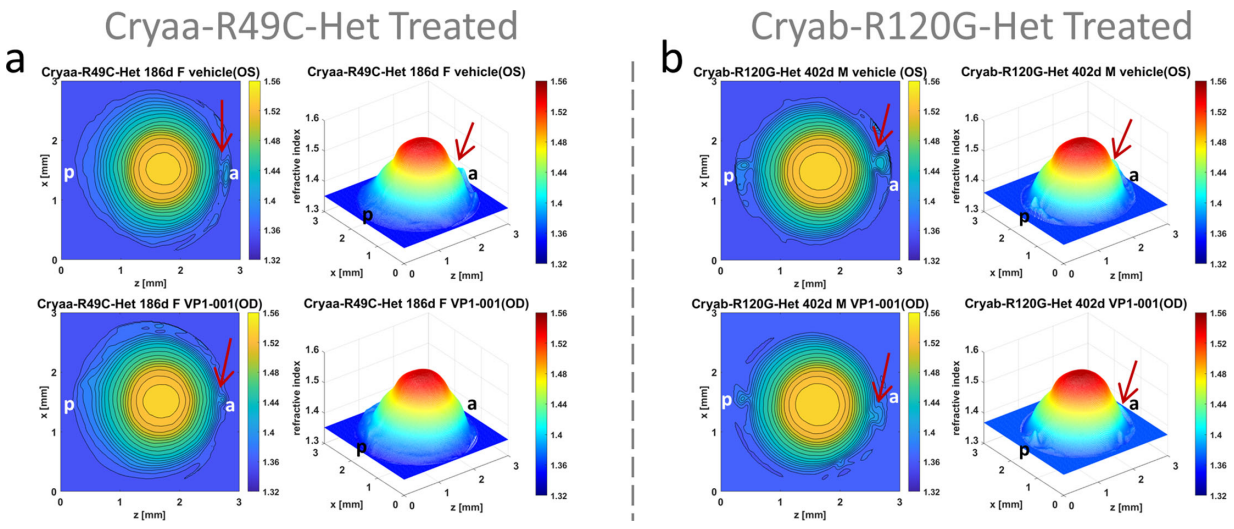

Figure 8. Refractive index profiles in *Cryaa*-R49C-Het eyes and *Cryab*-R120G-Het lenses. Refractive index distributions shown as contour plots in the mid-sagittal cross-sectional plane and as three-dimensional profiles in lenses from mice treated with vehicle in the OS eye and with VP1-001 in the OD eye: (**a**) *Cryaa*-R49C-Het mouse aged 186-days [ID 1237-7 Supplementary Table S1] and (**b**) *Cryab*-R120G-Het aged 402-days [ID 1144-6 Supplementary Table S1]. The polar regions of both vehicle treated lenses have small disturbances to the refractive index profile (indicated by *arrows*); these are slightly reduced in the VP1-001–treated lenses (indicated by *arrows*). a = anterior pole, p = posterior pole.

Investigative Ophthalmology & Visual Science

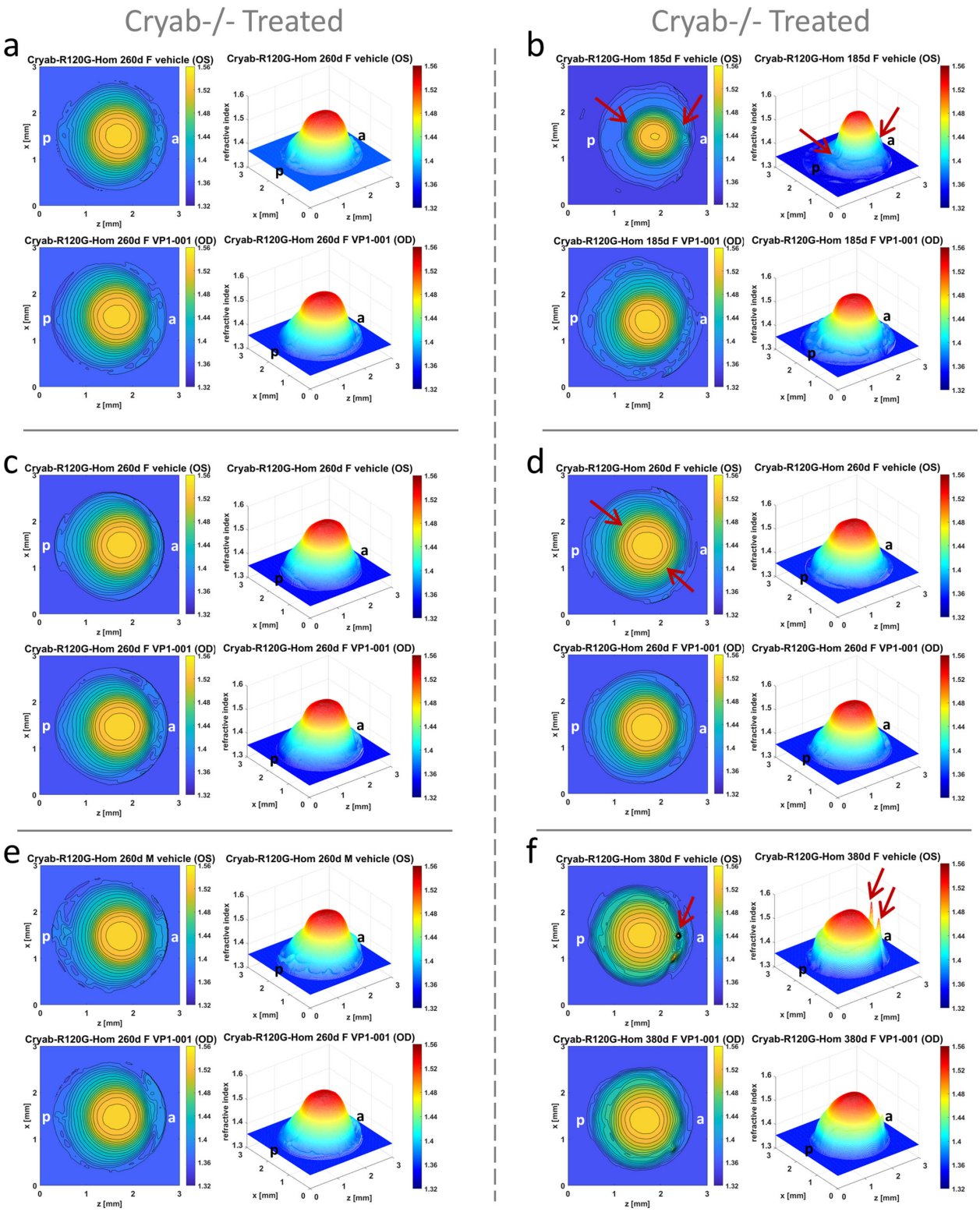

Figure 9. Refractive index profiles in *Cryab*-R120G-Hom lenses. Refractive index distributions shown as contour plots in the mid-sagittal cross-sectional plane and as 3-dimensional profiles in lenses in *Cryab*-R120G-Hom mouse treated with vehicle in the OS eye and with VP1-001 in the OD eye at (**a, c, d, e**) 260 days old [**a**: ID 1216-4, Supplementary Table S1; **c**: ID 1213-3 Supplementary Table S1; **d**:ID 1212-1 Supplementary Table S1], (**b**) 185 days old [ID 1231-4 Supplementary Table S1], and (**f**) 380 days old [ID 1150-4 Supplementary Table S1]. In the 260-day-old lenses (**a, c, e**) the refractive index profiles are skewed, and there is little if any difference between vehicle or VP1-001–treated lenses. Some small differences between lenses in the pair seen in (**d**) are apparent with irregularities in the refractive index contours in vehicle treated lens (indicated by the arrows) which are not present in the corresponding VP1-001–treated lens. There are greater differences evident in the 185-day-old (**b**) and 380-day-old lens pairs (**f**). In **b** the vehicle-treated 185-day-old lens has a narrow and asymmetric profile with a relatively sharp peak, an indentation in the contours and in the GRIN profile in the posterior polar region

Investigative Ophthalmology & Visual Science

(indicated by *arrows*), protruding contours and slight distortion in the GRIN profile in the anterior polar region (indicated by *arrows*). These are not seen in the VP1-001–treated lens (**b**) which manifests a profile closer in breadth to normal lenses, more regular contours. The 380-day-old lens in **f** shows localized peaks in refractive index indicative of protein aggregation in the vehicle-treated lens (indicated by *arrows*) that are not seen in the VP1-001–treated lens. a = anterior pole, p = posterior pole.

of the lens and hence clarity of vision. Detecting α-crystallin mutation-induced structural features by X-ray phase tomography could aid in the diagnosis, prognosis, or treatment of cataracts.

Several important aspects of the present study require further discussion. Identifying possible correlations of apparent cataract score with some of the refractive index profiles is critical yet there cannot be an expectation of a direct relationship between cataract grade from slit lamp images and refractive index. The slit lamp illuminates a section of the lens and if the traversing light encounters protein aggregates or other disturbances that cause refractive index fluctuations and hence light scatter, the lens will appear to be opacified. This can result in a relatively high cataract grading even if the aggregates are small and localized and the rest of the lens is not opacified; such a lens can have a relatively unperturbed refractive index profile. This would explain why there are differences in some of the slit-lamp images and the refractive index measurements such as observed when comparing WT lenses aged 493 and 738 days in Figures 1 and 2 and comparing the WT lens aged 493 days and the *Cryaa*-R49C-Het lenses in Figures 1 and 3. It should also be noted that with a slit-lamp examination, the observer only sees the light that is back-scattered and not the refracted image-forming light that reaches the retina. Quantification of the slit-lamp image using densitometric analysis can provide a more accurate grading.[47] However, a slit lamp image does not yield direct information about what the eye sees or how distorted the image may be on the retina. The refractive index profiles, conversely, do give an indication of the overall optics of the lens, showing regions through which light will be refracted and regions where light may be scattered. The refractive index measurements using X-ray phase tomography based on X-ray Talbot interferometry, the most accurate method currently available for measuring the refractive index of intact lenses[48] provide a detailed analysis of subtle fluctuations in protein concentrations and lens protein gradients, which are not detected by slit lamp images. Importantly, this technique allows for the quantitation of the refractive index and protein density distributions across the eye lens, as previously demonstrated in the murine lens.[32,35] Hence, although complementary in nature, comparing the results of these two methods on the same tissue cannot be expected to provide direct correspondence in all cases.

This notwithstanding, there is some consistency between refractive index measurements and slit lamp images in the results from mutant lenses. In the case of *Cryab*-R120G mutant lenses, changes in the lens periphery with light microscopy[15] correlated with changes in refractive index profiles found in the present study (Fig. 4). There was also evidence of correlation between slit lamp findings and refractive index measurements in lenses treated with VP1-001 and vehicle. Apparent cataract gradings from slit lamp images were, in all cases, lower in mice treated with VP1-001 compared to vehicle treated lens in the same pair (Table). This correlates with refractive index measurements in WT lenses of mice treated with VP1-001 which were less disturbed than in lenses treated with vehicle (Figs. 7b and 7d). The same was seen for *Cryaa*-R49C and *Cryab*-R120G heterozygous pairs (Fig. 8) and for some of the *Cryab*-R120G homozygous pairs (Fig. 9). It could be that newly differentiated lens fiber cells, which emerged during the course of VP1-001 treatment, adopt a normal structure and are overlaid on deformed cells or it could be indicative of an interaction between VP1-001 and lens fiber cells that restores structure for proper optical function. Such an interaction requires further investigation given the findings of Daszynski et al.,[49] whose crystallin solubility, molecular modeling, and docking studies did not show that oxysterols bind crystallin aggregates to reverse cataracts.[49] The disturbances in outer regions of the GRIN (Figs. 5c, 5f, 9f) that are decreased in lenses treated by VP1-001 (Fig. 9f) are likely to result from abnormalities in cellular modeling or other damage that cause localized spots of high protein density in these layers, rather than from protein aggregation such as seen in older lenses and central regions of the lens.

The other important entity for lens transparency and for a viable GRIN is water and more specifically, the regulation of its transport by aquaporins.[50,51] Water permeability of the most abundant of the aquaporins in the lens, aquaporin 0, is modified by lipid composition of the cell membrane bilayer.[52] Oxysterols are involved in cholesterol homeostasis and enzymatically produced side-chain oxysterols, have been shown to increase permeability of membranes.[53] It is plausible that the oxysterol VP1-001 could have interacted with aquaporin 0 in mutant lenses to alter membrane permeability and localized protein/water ratio and thereby improved the GRIN profile. Cataracts have been found to start from local disturbances to cell membranes;[54] any reversal of the process would likely be most effective if it occurred at the site of cataract formation (i.e., at or close to the membranes).

Cryab-R120G lenses, which are a model for human cataracts and myopathy, exhibited the greatest irregularities in their profiles surrounding the lens periphery particularly in the *Cryab*-R120G-Hom lenses. The profile peaks in lens nuclei represent tissue that has been laid down in early gestation, and the profile shapes in Figures 5b and 5e suggest that protein concentration may not be evenly distributed along the fiber cells. Deviations from a smooth GRIN were also seen in some profiles. These features suggest possible changes in the growth rate of the lens or in the complement of proteins laid down in the cells of the regions where these irregularities are found, which may represent different protein densities that have been labelled as zones of discontinuity.[55] Thus far, these zones have only been observed in lenses in the living human eyes. Although zones of discontinuity do not affect refraction or impair vision, they may indicate important stages in the growth and development of the lens[33] and therefore require further investigation. The most marked differences in the optics of the lens were seen in the *Cryab*-R120G-Hom lenses with VP1-001 treatment compared to their vehicle treated counterparts (Figs. 9b and 9f). The former manifested more regular refractive index profiles than the latter and this corresponded

Investigative Ophthalmology & Visual Science

to the results from slit lamp gradings (Table). Yet, whilst this mutant strain had the greatest response to VP1-001 treatment, not all lens pairs showed a difference between the VP1-001 and vehicle treated lenses. Given that the compounds were administered on the ocular surface, there may have been differences in uptake and the possibility that in some eyes the compound may have been diluted or even washed out by the tear layer.

In conclusion, X-ray phase tomography based on X-ray Talbot interferometry can distinguish subtle fluctuations in GRIN profiles in *Cryaa*-R49C and *Cryab*-R120G mutant lenses that other methods have been unable to detect. X-ray phase tomography can distinguish therapeutic changes induced by VP1-001 revealed by other methods using visible light, such as slit lamp biomicroscopy, and can localize these changes with greater precision. This advanced technique can provide very useful information about growth and development of the lens in the presence of a mutant chaperone protein, as well as offering future insights into their roles in other tissues, such as cardiac and skeletal muscle, where αB-crystallin is expressed. Future application should also include investigations into multilamellar bodies which have been found, from ultrastructural studies, in nuclei of normal lenses as well as in those with nuclear cataract with higher frequency in the latter.[56–58] These spherical entities, with multiple layers of lipid-rich membranes, vary from 1-4 microns in diameter[56–58] and, although relatively rare in frequency, are considered to be responsible for substantial proportion of light scattering in older and cataractous lenses because they create localized refractive index fluctuations.[56–58] Such insights will, in turn, advance knowledge about lens ultrastructure, biological function and optical performance and what may alter with other known crystallin mutations,[42] and water transport and could ultimately aid in the design of drugs to delay or inhibit cataract development.

Acknowledgments

The authors thank Stephanie Bozeman for technical assistance and Dr Leah Makley from Viewpoint Therapeutics who provided the VP1-001 and vehicle used in this study.

Supported by the National Institutes of Health (Grants EY05681-33, EY02687, and EY026474-01), Beamtime grants from SPring-8 synchrotron, Japan (Grants 2017A1197, 2018A1105, 2019A1115, 2019A1335), National Natural Science Foundation of China (Grant 82000878).

Disclosure: **K. Wang,** None; **M. Hoshino,** None; **K. Uesugi,** None; **N. Yagi,** None; **B.K. Pierscionek,** None; **U.P. Andley,** None

References

1. Bloemendal H, de Jong W, Jaenicke R, Lubsen NH, Slingsby C, Tardieu A. Ageing and vision: structure, stability and function of lens crystallins. *Prog Biophys Mol Biol*. 2004;86:407–485.
2. Pierscionek BK, Regini JW. The gradient index lens of the eye: an opto-biological synchrony. *Prog Retin Eye Res*. 2012;31:332–349.
3. Horwitz J. Alpha-crystallin can function as a molecular chaperone. *Proc Natl Acad Sci USA*. 1992;89:10449–10453.
4. Aquilina JA, Benesch JL, Bateman OA, Slingsby C, Robinson CV. Polydispersity of a mammalian chaperone: mass spectrometry reveals the population of oligomers in alphaB-crystallin. *Proc Natl Acad Sci USA*. 2003;100:10611–10616.
5. Horwitz J. The function of alpha-crystallin in vision. *Semin Cell Dev Biol*. 2000;11:53–60.
6. Andley UP, Malone JP, Townsend RR. In vivo substrates of the lens molecular chaperones alphaA-crystallin and alphaB-crystallin. *PLoS One*. 2014;9(4):e95507.
7. Derham BK, Harding JJ. Alpha-crystallin as a molecular chaperone. *Prog Retin Eye Res*. 1999;18:463–509.
8. Horwitz J. Alpha-crystallin. *Exp Eye Res*. 2003;76:145–153.
9. Andley UP, Hamilton PD, Ravi N. Mechanism of insolubilization by a single-point mutation in alphaA-crystallin linked with hereditary human cataracts. *Biochemistry*. 2008;47:9697–9706.
10. Cheng C, Xia CH, Huang Q, Ding L, Horwitz J, Gong X. Altered chaperone-like activity of alpha-crystallins promotes cataractogenesis. *J Biol Chem*. 2010;285:41187–41193.
11. Perng MD, Cairns L, van den IP, Prescott A, Hutcheson AM, Quinlan RA. Intermediate filament interactions can be altered by HSP27 and alphaB-crystallin. *J Cell Sci*. 1999;112(Pt 13):2099–2112.
12. Vicart P, Caron A, Guicheney P, et al. A missense mutation in the alphaB-crystallin chaperone gene causes a desmin-related myopathy. *Nat Genet*. 1998;20:92–95.
13. Mackay DS, Andley UP, Shiels A. Cell death triggered by a novel mutation in the alphaA-crystallin gene underlies autosomal dominant cataract linked to chromosome 21q. *Eur J Hum Genet*. 2003;11:784–793.
14. Bova MP, Yaron O, Huang Q, et al. Mutation R120G in alphaB-crystallin, which is linked to a desmin-related myopathy, results in an irregular structure and defective chaperone-like function. *Proc Natl Acad Sci USA*. 1999;96:6137–6142.
15. Andley UP, Hamilton PD, Ravi N, Weihl CC. A knock-in mouse model for the R120G mutation of alphaB-crystallin recapitulates human hereditary myopathy and cataracts. *PLoS One*. 2011;6(3):e17671.
16. Biswas A, Miller A, Oya-Ito T, Santhoshkumar P, Bhat M, Nagaraj RH. Effect of site-directed mutagenesis of methylglyoxal-modifiable arginine residues on the structure and chaperone function of human alphaA-crystallin. *Biochemistry*. 2006;45:4569–4577.
17. Truscott RJ, Friedrich MG. The etiology of human age-related cataract. Proteins don't last forever. *Biochim Biophys Acta*. 2016;1860(1 Pt B):192–198.
18. Truscott RJ. Age-related nuclear cataract-oxidation is the key. *Exp Eye Res*. 2005;80:709–725.
19. Andley UP. Crystallins in the eye: function and pathology. *Prog Retin Eye Res*. 2007;26:78–98.
20. Pierscionek BK, Augusteyn RC. Structure/function relationship between optics and biochemistry of the lens. *Lens Eye Toxic Res*. 1991;8(2-3):229–243.
21. Nakao S, Fujimoto S, Nagata R, Iwata K. Model of refractive-index distribution in the rabbit crystalline lens. *J Opt Soc Am*. 1968;58:1125–1130.
22. Palmer DA, Sivak J. Crystalline lens dispersion. *J Opt Soc Am*. 1981;71:780–782.
23. Campbell MC. Measurement of refractive index in an intact crystalline lens. *Vision Res*. 1984;24:409–415.
24. Pierscionek BK. Growth and ageing effects on the refractive index in the equatorial plane of the bovine lens. *Vision Res*. 1989;29:1759–1766.
25. Pierscionek BK. The refractive index along the optic axis of the bovine lens. *Eye*. 1995;9(Pt 6):776–782.
26. Pierscionek BK. Refractive index contours in the human lens. *Exp Eye Res*. 1997;64:887–893.

27. Moffat BA, Atchison DA, Pope JM. Age-related changes in refractive index distribution and power of the human lens as measured by magnetic resonance micro-imaging in vitro. *Vision Res*. 2002;42:1683–1693.
28. Jones CE, Pope JM. Measuring optical properties of an eye lens using magnetic resonance imaging. *Magn Reson Imaging*. 2004;22(2):211–220.
29. Jones CE, Atchison DA, Meder R, Pope JM. Refractive index distribution and optical properties of the isolated human lens measured using magnetic resonance imaging (MRI). *Vision Res*. 2005;45:2352–2366.
30. Lahm D, Lee LK, Bettelheim FA. Age dependence of freezable and nonfreezable water content of normal human lenses. *Invest Ophthalmol Vis Sci*. 1985;26:1162–1165.
31. Momose A, Kawamoto S, Koyama I, Hamaishi Y, Takai K, Suzuki Y. Demonstration of X-Ray Talbot interferometry. *Jpn J Appl Phys*. 2003;42(7b):L866–L868.
32. Hoshino M, Uesugi K, Yagi N, Mohri S, Regini J, Pierscionek B. Optical properties of in situ eye lenses measured with X-ray Talbot interferometry: a novel measure of growth processes. *PLoS One*. 2011;6(9):e25140.
33. Bahrami M, Hoshino M, Pierscionek B, Yagi N, Regini J, Uesugi K. Optical properties of the lens: an explanation for the zones of discontinuity. *Exp Eye Res*. 2014;124:93–99.
34. Wang K, Vorontsova I, Hoshino M, et al. Aquaporins have regional functions in development of refractive index in the zebrafish eye lens. *Invest Opthal Vis Sci*. 2021;62:23.
35 Cheng C, Parreno J, Nowak RB, et al. Age-related changes in eye lens biomechanics, morphology, refractive index and transparency. *Aging*. 2019;11:12497.
36. Kroger RH, Campbell MC, Fernald RD. The development of the crystalline lens is sensitive to visual input in the African cichlid fish, Haplochromis burtoni. *Vision Res*. 2001;41(5):549–559.
37. Makley LN, McMenimen KA, DeVree BT, et al. Pharmacological chaperone for alpha-crystallin partially restores transparency in cataract models. *Science*. 2015;350(6261):674–677.
38. Kolling FRC, IV, Wallace M, Andley UP. Genomic analysis of *Cryaa*-R49C and *Cryab*-R120G knockin mutant mice: 10 year follow-up. *J Clin Exp Ophthalmol*. 2021;12:1–6.
39. Molnar KS, Dunyak BM, Su B, et al. Mechanism of action of VP1-001 in cryAB(R120G)-associated and age-related cataracts. *Invest Ophthalmol Vis Sci*. 2019;60:3320–3331.
40. Mackay DS, Andley UP, Shiels A. A missense mutation in the gammaD crystallin gene (CRYGD) associated with autosomal dominant "coral-like" cataract linked to chromosome 2q. *Mol Vis*. 2004;10:155–162.
41. Moore AT. Understanding the molecular genetics of congenital cataract may have wider implications for age related cataract. *Br J Ophthalmol*. 2004;88:2–3.
42. Andley UP. Crystallins and hereditary cataracts: molecular mechanisms and potential for therapy. *Expert Rev Mol Med*. 2006;8(25):1–19.
43. Wang K, Hoshino M, Uesugi K, Yagi N, Young RD, Frost BE, et al. Cell compaction is not required for the development of gradient refractive index profiles in the embryonic chick lens. *Exp Eye Res*. 2020;197:108112.
44. Uesugi K, Hoshino M, Yagi N. Comparison of lens- and fiber-coupled CCD detectors for X-ray computed tomography. *J Synchrotron Radiat*. 2011;18(Pt 2):217–223.
45. Andley UP, Tycksen E, McGlasson-Naumann BN, Hamilton PD. Probing the changes in gene expression due to alpha-crystallin mutations in mouse models of hereditary human cataract. *PLoS One*. 2018;13(1):e0190817.
46. Frankfater C, Bozeman SL, Hsu FF, Andley UP. Alpha-crystallin mutations alter lens metabolites in mouse models of human cataracts. *PLoS One*. 2020;15(8):e0238081.
47. Kunze S, Dalke C, Fuchs H, et al. New mutation in the mouse Xpd/Ercc2 gene leads to recessive cataracts. *PLoS One*. 2015;10(5):e0125304.
48. Pierscionek BK, Bahrami M, Hoshino M, Uesugi K, Regini J, Yagi N. The eye lens: age-related trends and individual variations in refractive index and shape parameters. *Oncotarget*. 2015;6:30532–30544.
49. Daszynski DM, Santhoshkumar P, Phadte AS, et al. Failure of oxysterols such as lanosterol to restore lens clarity from cataracts. *Sci Rep*. 2019;9:8459.
50. Verkman AS, Ruiz-Ederra J, Levin MH. Functions of aquaporins in the eye. *Progr Retin Eye Res*. 2008; 27: 420–433.
51. Schey KL, Wang Z, Wenke JL, Qi Y. Aquaporins in the eye: expression, function, and roles in ocular disease. *Biochim Biophys Acta*. 2014; 1840: 1513–1523.
52. Tong J, Canty JT, Briggs MM, McIntosh TJ. The water permeability of aquaporin-0 depends on its lipid bilayer environment. *Exp Eye Res*. 2013;113:32–40.
53. Olsen BN, Schlesinger PH, Ory DS, Baker NA. Side-chain oxysterols: from cells to membranes to molecules. *Biochim Biophys Acta*. 2012;1818:330–336.
54. Duindam JJ, Vrensen GFJM, Otto C, Greve J. Cholesterol, phospholipid, and protein changes in focal opacities in the human eye lens. *Invest Ophthalmol Vis Sci*. 1998;39:94–103.
55. Koretz JF, Cook CA, Kuszak JR. The zones of discontinuity in the human lens: development and distribution with age. *Vision Res*. 1994;34:2955–2962.
56. Gilliland KO, Freel CD, Lane CW, Fowler WC, Costello MJ. Multilamellar bodies as potential scattering particles in human age-related nuclear cataracts. *Mol Vis*. 2001;7:120–130.
57. Gilliland KO, Freel CD, Johnsen S, Fowler WC, Costello MJ. Distribution, spherical structure and predicted Mie scattering of multilamellar bodies in human age-related nuclear cataracts. *Exp Eye Res*. 2004;79:563–576.
58. Costello MJ, Johnsen S, Gilliland KO, Freel CD, Fowler WC. Predicted Light Scattering from Particles Observed in Human Age-Related Nuclear Cataracts Using Mie Scattering Theory. *Invest Ophthalmol Vis Sci*. 2007;48:303–312.

Investigative Ophthalmology & Visual Science